Nonlinear Programming Hybrid Beam-Column Element Formulation for Large-Displacement Elastic and Inelastic Analysis

C. P. Andriotis[1]; K. G. Papakonstantinou, M.ASCE[2]; and V. K. Koumousis, M.ASCE[3]

Abstract: Modern structural analysis necessitates numerical formulations with advanced nonlinear attributes. To that end, numerous finite elements have been proposed, spanning from classical to hybrid standpoints. In addition to their individual features, all formulations originally stem from an underlying variational principle, which can be deemed as a unified energy metric of the system. The corresponding equations of structural equilibrium define a stationary point of the assumed principle. Following this logic in this work, the total potential energy is directly treated as an objective function, subject to some kinematic compatibility constraints, within the conceptions of nonlinear programming. The only approximated internal field is curvature, whereas displacements occur solely as nodal entities and Lagrange multipliers serve compatibility. Thereby, a new nonlinear programming hybrid element formulation is derived, which uses exact kinematic fields, can incorporate nonlinear assumptions of any extent, and is amenable to various applicable nonlinear programming algorithms. The suggested nonlinear program is presented in detail herein, together with its consistent second-order iterative solution procedure. The results obtained in benchmark nonlinear structural problems are validated and compared with OpenSees flexibility-based elements, showcasing notable performance in terms of accuracy, mesh density discretization, computational speed, and robustness. **DOI: 10.1061/(ASCE)EM.1943-7889.0001483.**

Introduction

Structural systems subject to multiple natural or anthropogenic hazards are often required to endure extreme event loads that can drive them to highly nonlinear regimes. Accordingly, structural element models have to support highly nonlinear simulations that capture materially and geometrically nonlinear responses effectively in order to enable realistic structural assessments. To accomplish this, structural element models and relevant numerical procedures should aim at concurrently satisfying the notions of (i) accuracy, (ii) coarse mesh discretization, (iii) computational speed, and (iv) robust algorithmic performance. All these attributes are of great importance in any type of structural analysis and, to the extent they are combined, form the key for high-performance nonlinear and collapse simulations.

Current structural analysis trends are shifting from deterministic to probabilistic approaches in order to embrace the notions of uncertainty, risk, and reliability (Au and Beck 2001; Baker 2015; Andriotis and Papakonstantinou 2018). Additionally, in recent efforts toward viable optimum decision planning, the engineering community uses large scale optimization formulations with multiple objectives and constraints, as well as advanced life-cycle analyses. All these challenging analysis tasks demand multiple computational runs and robust algorithms; hence, the underlying numerical models are required to provide computational speed and remedy premature algorithmic stops without sacrificing accuracy. The need for capturing nonlinearities realistically and reliably is also of paramount importance in distinct extreme-scenario analyses. In progressive collapse analysis, for example, where scenarios such as sudden loss of columns are investigated, the system has to reach an alternative equilibrium point leveraging catenary mechanisms triggered by large displacements and rotations (Izzuddin et al. 2008; Gerasimidis et al. 2015). In response to these challenges, research efforts from displacement-based to hybrid standpoints have managed to significantly advance the efficacy of nonlinear analyses, proposing various structural element formulations and improved algorithms. Nonetheless, in general, the various formulations and computational tools still have certain limitations, which are particularly prominent in problems with highly nonlinear characteristics, either through problematic convergence, premature analysis stops, or inaccurate equilibrium branches.

In displacement-based approaches of beam-column elements, strains are generally derived by Hermitian polynomial shape functions that interpolate the displacement field (Argyris et al. 1964; Bathe and Bolourchi 1979). This concept satisfies compatibility but trades off equilibrium in inelastic and large displacement problems. Polynomial interpolation introduces field inconsistencies in this formulation, locking phenomena emerge, and even dense meshes are often practically insufficient to obtain accurate responses, or the solutions may converge very slowly (Alemdar and White 2005). Techniques of underintegration or selective integration, implemented to prevent locking, can cause spurious modes that lead to numerical instabilities (De Borst et al. 2012). Overall, displacement-based formulations for inelastic problems with large displacements are computationally intensive and are susceptible to premature analysis termination and deteriorated algorithmic performance.

[1]Ph.D. Candidate, Dept. of Civil and Environmental Engineering, Pennsylvania State Univ., University Park, PA 16802 (corresponding author). Email: cxa5246@psu.edu; charandriotis@gmail.com

[2]Assistant Professor, Dept. of Civil and Environmental Engineering, Pennsylvania State Univ., University Park, PA 16802.

[3]Professor, Dept. of Civil and Environmental Engineering, National Technical Univ. of Athens, Athens 15780, Greece.

Note. This manuscript was submitted on September 27, 2017; approved on January 23, 2018; published online on August 2, 2018. Discussion period open until January 2, 2019; separate discussions must be submitted for individual papers. This paper is part of the ***Journal of Engineering Mechanics***, © ASCE, ISSN 0733-9399.

Force-based approaches suggest a complementary formulation instead. Rather than interpolating the displacement field, force shape functions are introduced in the expression for the principle of virtual forces (Zeris and Mahin 1988). Inherently satisfying equilibrium, force-based elements derive accurate results in elastoplastic analysis of beam-column structures without geometrical nonlinearities (Taucer et al. 1991). Fine discretization is avoided in this class of applications and the computational cost drops drastically in comparison to displacement-based analysis. However, in large displacement problems, the accuracy of flexibility-based analysis depends on discretization, despite the fact that noticeable expansions have managed to reduce the mesh density (Neuenhofer and Filippou 1998; De Souza 2000). Discretization is required in order for field inconsistencies due to bending and membrane modes coupling to be moderated, which increases the computational cost significantly in highly geometrically nonlinear problems. Additionally, the adopted corotational transformation, implemented to exclude rigid body modes, can introduce important rotational limitations that can potentially lead to early analysis termination or prevent realistic results (Neuenhofer and Filippou 1998; Felippa and Haugen 2005).

Mixed beam-column elements combine characteristics of both stiffness-based and flexibility-based approaches. Shape functions are introduced in both displacement and force fields in the standard mixed approach (Spacone et al. 1996). These elements are also called multifield elements and their state determination technically stems from the Hellinger-Reissner and Hu-Washizu variational principles (Felippa 1994). The main reason behind the development of mixed elements is the remedy of various shortcomings emerging in single-field formulations, such as dense mesh requirements in highly nonlinear problems and locking effects caused by field inconsistencies (Stolarski and Belytschko 1983; Taylor et al. 2003; Alemdar and White 2005; Saritas and Filippou 2009; Soydas and Saritas 2013). However, variations in multiple internal fields imply that the structural degrees of freedom (DOFs) may increase, something that can outweigh the benefits in conjunction with the dense mesh discretization that is still required in highly nonlinear problems. Overall, it has been observed that for a given level of accuracy, superiority of mixed elements is not always apparent and a similar computational effort as for other elements is often required (Hjelmstad and Taciroglu 2003).

Hybrid element approaches are similar to mixed approaches, including, however, additional variables that do not necessarily correspond to internal fields, for example, Lagrange multipliers. Lagrange multipliers can be used for plasticity, stress continuity, or kinematic considerations (Sivaselvan and Reinhorn 2006; Santos and Moitinho de Almeida 2010; Saje et al. 1997). In general, hybrid elements have shown noticeable performance in curing locking problems (Stolarski and Belytschko 1983), yet in some cases the various formulations rather increase the DOFs compared to flexibility-based elements, while also maintaining the need for fine discretization.

Some kinematic approaches are also referred to as "geometrically exact" or "strain-based" in the literature. These formulations can essentially be classified as either hybrid or mixed because they fall into the generic category of multifield methods. Exact formulations, however, do not adopt corotational transformations or any kinematic simplifications, having the capability to model arbitrarily large displacements and rotations for highly nonlinear problems (Saje et al. 1997; Santos et al. 2011). Recent and past research efforts investigate similar methodologies further, also within the framework of quadrature weak forms (Zhang and Zhong 2013).

In an effort to address these issues in a unified context and motivated by the conceptions of hybrid methodologies and geometrically exact formulations, the present work primarily aims at posing the problem in an alternative statement. Structural analysis is straightforwardly cast in the framework of optimization and can be eventually carried out as a pure nonlinear programming (NLP) problem. The total potential energy (TPE) is minimized on the basis of primal and dual optimization considerations, whereas compatibility constraints are appended via Lagrange multipliers to the discretized TPE functional, which serves as the objective function of the problem. With this TPE hybridization nonlinear kinematic relations are fully incorporated without any sort of simplifications in the deformation variables. Material nonlinearities are introduced along the premises of fiber discretization, which allows for distributed plasticity along the element and over the cross-sections to be accounted for. Displacements and rotations, along with strains within the element, define the set of primal variables, and technically the solution procedure seeks their optimal values in terms of energy. The formulation eventually renders displacements as pure nodal variables; therefore, in contrast to curvature, they are not internal fields and thus not interpolated. The derived NLP hybrid element controls to a great extent the global structural response at the element level and, as such, the number of DOFs is significantly reduced in comparison to flexibility-based approaches, as also shown in detail in the demonstration and discussion of the numerical results.

Nonlinear Programming Problem Statement

In this section, the suggested NLP problem statement is presented. In an effort to alleviate the notational complexities, all derivations are developed for a single element. The extension to multiple elements is straightforward, following standard finite-element assembly methods. As per the NLP form considered, the element formulation follows the general problem statement (Bazaraa et al. 2006):

$$\min_{\mathbf{z}} f(\mathbf{z}) \quad \text{s.t. } \mathbf{z} \in Z = \{\mathbf{z}: \mathbf{h}(\mathbf{z}) = \mathbf{0}, \mathbf{g}(\mathbf{z}) \le \mathbf{0}\} \tag{1}$$

where f = TPE objective function; $\mathbf{z}$ = vector of all sought variables; $\mathbf{h}$ = set of equality constraints, pertaining, for example, to kinematic relations or master-slave node sets; and $\mathbf{g}$ = set of inequality constraints, accounting, for example, for structural pounding or contact considerations. Herein, we are restricted to the essential equality constraints that guarantee the kinematic compatibility but the generic form of Eq. (1) implies the capability of augmenting the nature of the constraints with respect to any potential problem-dependent requirements.

Kinematic Equality Constraints

The axial deformation ε in the deformed configuration of the beam can be derived by the rotated engineering strain (Crisfield 1997), which is defined as follows:

$$\varepsilon = \frac{ds - dx}{dx} \tag{2}$$

where the infinitesimal lengths ds, dx refer to the current and initial configuration, respectively. Consistent with the geometry of the deformed shape, the following kinematic relations can be derived:

$$\sin\theta = \frac{dv}{(\varepsilon + 1)dx} \tag{3}$$

$$\cos\theta = \frac{du + dx}{(\varepsilon + 1)dx} \tag{4}$$

where u, v, and θ designate the horizontal and vertical displacements and rotation fields along the element length, respectively, in a standard Cartesian system. In addition, along the lines of Euler-Bernoulli beam theory assumptions, curvature κ can be defined as:

$$\kappa = \frac{d\theta}{dx} \tag{5}$$

Integrating Eqs. (3)–(5) along the length L of the element, we derive the expressions of the Reissner beam theory (Reissner 1972), without taking into account shear deformations:

$$q_4 - q_1 = \int_0^L [(\varepsilon + 1)\cos\theta - 1]dx \tag{6}$$

$$q_5 - q_2 = \int_0^L (\varepsilon + 1)\sin\theta dx \tag{7}$$

$$q_6 - q_3 = \int_0^L \kappa dx \tag{8}$$

where $\mathbf{q} = [\,q_1 \quad q_2 \quad q_3 \quad q_4 \quad q_5 \quad q_6\,]$, $[\,q_1 \quad q_2 \quad q_3\,] = \mathbf{u}(0)$, and $[\,q_4 \quad q_5 \quad q_6\,] = \mathbf{u}(L)$ for $\mathbf{u} = [\,u \quad v \quad \theta\,]$, in accordance with Fig. 1. The integrals of Eqs. (6)–(8) can be numerically evaluated by any Gaussian-type quadrature. The type of quadrature suggests the number and location of the colocation points, that is, colocation points are chosen so that they coincide with the quadrature points. Thereby, the zero equality constraints are obtained:

$$\mathbf{h}^A = \begin{bmatrix} q_4 - q_1 - \sum_{i=1}^n c_i(\varepsilon_i + 1)\cos\theta_i + L \\ q_5 - q_2 - \sum_{i=1}^n c_i(\varepsilon_i + 1)\sin\theta_i \\ q_6 - q_3 - \sum_{i=1}^n c_i\kappa_i \end{bmatrix} \tag{9}$$

where c_i = weights of the numerical integration; and n = number of quadrature points. Rotation $\theta_i = \theta(x_i)$ at each colocation point is connected to curvature as a result of integrating Eq. (5). Introducing Lagrangian polynomials to interpolate curvature of the quadrature points, the respective integral from $x = 0$ to $x = x_i$ gives:

$$\theta_i = q_3 + \sum_{j=1}^n \Theta_{ij}\kappa_j \tag{10}$$

$$\mathbf{\Theta} = L\begin{bmatrix} \xi_1 & \frac{\xi_1^2}{2} & \cdots & \frac{\xi_1^n}{n} \\ \vdots & \vdots & \ddots & \vdots \\ \xi_n & \frac{\xi_n^2}{2} & \cdots & \frac{\xi_n^n}{n} \end{bmatrix}\mathbf{G}^{-1}, \qquad \mathbf{G} = \begin{bmatrix} 1 & \xi_1 & \xi_1^2 & \cdots & \xi_1^{n-1} \\ \vdots & \vdots & \vdots & \ddots & \vdots \\ 1 & \xi_n & \xi_n^2 & \cdots & \xi_n^{n-1} \end{bmatrix} \tag{11}$$

where $\xi = \frac{x}{L}$; and $\mathbf{G}$ = Vandermonde matrix. This is a convenient way to write θ_i as a function of the curvature values at the integration points, as similarly implemented in De Souza (2000) for a curvature-based displacement interpolation. From Eq. (10), the second set of equality constraints is derived:

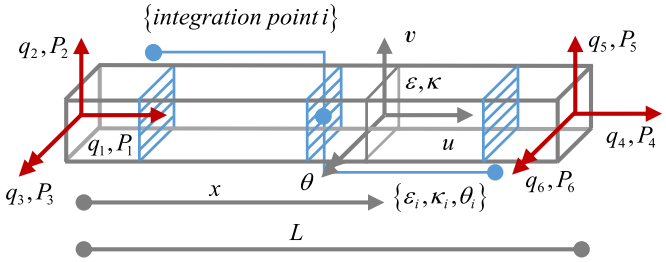

Fig. 1. Element variables and internal fields.

$$\mathbf{h}^B = \begin{bmatrix} \theta_1 - q_3 - \sum_{j=1}^n \Theta_{1j}\kappa_j \\ \vdots \\ \theta_n - q_3 - \sum_{j=1}^n \Theta_{nj}\kappa_j \end{bmatrix} \tag{12}$$

Combining Eqs. (9) and (12), we have:

$$\mathbf{h}(\mathbf{z}) = \begin{bmatrix} \mathbf{h}^A \\ \mathbf{h}^B \end{bmatrix} = \mathbf{0} \tag{13}$$

where $\mathbf{z} = \begin{bmatrix} \{\mathbf{y}_i\}_{i=1}^n \\ \mathbf{q} \end{bmatrix}$, $\mathbf{y}_i^T = [\,\varepsilon_i \quad \kappa_i \quad \theta_i\,]$. The equality constraints defined in Eq. (9) are nonlinear, except the last one, whereas all the constraints in Eq. (12) are linear. This is an important note because linear constraints can be leveraged in order to restrict iterates of the numerical procedure in the corresponding feasible hyperplane, as shown in more detail in the next section.

Objective Function and Lagrangian

Variational principles are the cornerstones of finite element analysis because they mathematically relate physical properties of structural systems to a scalar. The TPE functional of an individual element, assuming only nodal loads, can be written as:

$$\Pi = \int_0^L W(\varepsilon, \kappa)dx - \mathbf{P}^T\mathbf{q} \tag{14}$$

where $\mathbf{P}$ designates the vector of external nodal forces for each element, as in Fig. 1; and $W(\varepsilon, \kappa)$ = strain energy per unit reference length such that:

$$\frac{\partial W(\varepsilon, \kappa)}{\partial \varepsilon} = N, \qquad \frac{\partial W(\varepsilon, \kappa)}{\partial \kappa} = M \tag{15}$$

where N, M = axial force and bending moment, respectively. A discrete representation of Eq. (14) can be given by numerically computing the involved integral:

$$f(\mathbf{z}) = \sum_{i=1}^n c_i W(\varepsilon_i, \kappa_i) - \mathbf{P}^T\mathbf{q} \tag{16}$$

Eqs. (16) and (13) constitute the primal constrained NLP problem, as presented in Eq. (1). We can now hybridize the energy functional of Eq. (16), attaching the equality constraints to the objective, by introducing the Lagrange multipliers $\boldsymbol{\lambda} = \begin{bmatrix} \boldsymbol{\lambda}^A \\ \boldsymbol{\lambda}^B \end{bmatrix}$. Thereby, the Lagrangian of the problem is obtained:

$$f_h(\mathbf{z}, \boldsymbol{\lambda}) = \sum_{i=1}^n c_i W(\varepsilon_i, \kappa_i) - \mathbf{P}^T\mathbf{q} + \boldsymbol{\lambda}^T\mathbf{h}(\mathbf{z}) \tag{17}$$

Eq. (17) involves displacements and rotations, strains, and Lagrange multipliers as unknown variables, thus sharing common features with the three-field Hu-Washizu principle. However, in

contrast to standard mixed approaches that are based on this and similar principles, in this formulation displacements are not internal fields and Lagrange multipliers cannot be directly associated with certain stress resultants in order to be interpolated through shape functions.

Standardized NLP Hybrid Element Formulation

The compactly described problem in Eq. (17) can be solved by a variety of nonlinear programming solvers. However, deriving a solution procedure compatible with Newton-type schemes that are favorably implemented in standard structural software packages is the particular focus of this work. Structural analysis software packages mainly use the direct stiffness concept to assemble global structural matrices. Therefore, determining the element state at each step is required. Before the element state determination, processing at the cross-section level has to be conducted so that the tangential properties of the element are quantified. This task is performed here by means of fiber discretization, which facilitates distributed plasticity considerations along the element and over the cross-sections.

Cross-Section Fiber Discretization

Following the Euler-Bernoulli beam theory assumptions for plane cross-sections, the strain at each individual fiber can be determined as:

$$\varepsilon_f = \varepsilon - y_f \kappa \tag{18}$$

where y_f = distance of the centroid of the beam to each individual fiber. In relation to Eq. (15), the stress resultants N, M can be calculated. As a result, the gradients of strain energy, which are later used in the iterative process, can be readily obtained. Due to the fiber discretization of the cross-sections, the corresponding sectional integrals that provide the stress resultants are computed by the midpoint rule as:

$$\begin{bmatrix} N \\ M \end{bmatrix} = \begin{bmatrix} \sum_{i=1}^{n_f} A_i \sigma_{fi} & \sum_{i=1}^{n_f} A_i y_{fi} \sigma_{fi} \end{bmatrix}^T \tag{19}$$

where n_f = number of fibers; σ_{fi} = stress of fiber i; and A_i = corresponding area. The tangent stiffness of the cross-section, which is later used for determining the second-order gradients of $W(\varepsilon, \kappa)$, is computed by:

$$\mathbf{k}_{sec} = \begin{bmatrix} \sum_{i=1}^{n_f} E_i^t A_i & -\sum_{i=1}^{n_f} E_i^t A_i y_{fi} \\ -\sum_{i=1}^{n_f} E_i^t A_i y_{fi} & \sum_{i=1}^{n_f} E_i^t A_i y_{fi}^2 \end{bmatrix} \tag{20}$$

Section fibers may follow any one-dimensional constitutive law, which complies with their individual material properties and captures nonlinearities prompted by elastic-plastic deformations and potential damage effects, as for example in Andriotis et al. (2015).

Element State Determination

The Lagrangian in Eq. (17) can be considered the new unconstrained objective of the NLP problem, containing both primal and dual components. The Karush-Kuhn-Tucker necessary optimality conditions describe a stationary point of the hybridized potential, given by:

$$\nabla f_h^T = \begin{bmatrix} \{\nabla_{\mathbf{y}_i} f_h\}_{i=1}^n \\ \nabla_{\mathbf{q}} f_h \\ \nabla_{\boldsymbol{\lambda}} f_h \end{bmatrix} = 0 \tag{21}$$

Using Eqs. (13) and (15) the equations of the stationary point of Eq. (21) can be written in more detail as:

$$\left.\begin{array}{l} N_i = \lambda_1^A \cos\theta_i + \lambda_2^A \sin\theta_i \\ M_i = \lambda_3^A + \dfrac{1}{c_i} \displaystyle\sum_{j=1}^{n} \Theta_{ji} \lambda_j^B \\ \lambda_i^B = c_i(\varepsilon_i + 1)(\lambda_2^A \cos\theta_i - \lambda_1^A \sin\theta_i) \end{array}\right\}_{i=1}^{n} \tag{22}$$

$$\nabla_{\mathbf{q}} \mathbf{h} \boldsymbol{\lambda} = \mathbf{P} \tag{23}$$

$$\mathbf{h} = \mathbf{0} \tag{24}$$

where, as Eq. (23) implies, matrix $\nabla_{\mathbf{q}} \mathbf{h}$ is the constant transformation matrix from Lagrange multipliers to nodal forces, given by:

$$\nabla_{\mathbf{q}} \mathbf{h} = [\nabla_{\mathbf{q}} \mathbf{h}^A \quad \nabla_{\mathbf{q}} \mathbf{h}^B], \qquad \nabla_{\mathbf{q}} \mathbf{h}^A = \begin{bmatrix} -1 & 0 & 0 & 1 & 0 & 0 \\ 0 & -1 & 0 & 0 & 1 & 0 \\ 0 & 0 & -1 & 0 & 0 & 1 \end{bmatrix}^T,$$
$$\nabla_{\mathbf{q}} \mathbf{h}^B = \begin{bmatrix} 0 & 0 & -1 & 0 & 0 & 0 \\ \vdots & \vdots & \vdots & \vdots & \vdots & \vdots \\ 0 & 0 & -1 & 0 & 0 & 0 \end{bmatrix}^T \tag{25}$$

Moreover, $\nabla_{\lambda} f_h$ is essentially a restatement of the compatibility constraints established in Eq. (13). Eqs. (22)–(24) show that the mathematical form of equilibrium is a set of nonlinear algebraic equations, which can be linearized between two successive steps k and $k+1$, so that the Newton's direction of descent $\mathbf{d_z}$ is computed:

$$\underbrace{\begin{bmatrix} \nabla_{\mathbf{yy}}^2 f_h^k & \mathbf{0} & \nabla_{\mathbf{y}} \mathbf{h}^k \\ & \mathbf{0} & \nabla_{\mathbf{q}} \mathbf{h}^k \\ \text{symm.} & & \mathbf{0} \end{bmatrix}}_{\mathbf{H}^k} \underbrace{\begin{bmatrix} \mathbf{d_y}^k \\ \mathbf{d_q}^k \\ \mathbf{d_\lambda}^k \end{bmatrix}}_{\mathbf{d_z}^k} + \underbrace{\begin{bmatrix} \nabla_{\mathbf{y}} f_h^k \\ \nabla_{\mathbf{q}} f_h^k \\ \mathbf{h}^k \end{bmatrix}}_{\nabla f_h^k} = \mathbf{0} \tag{26}$$

where $\mathbf{H}^k$ = tangential Hessian matrix of the element, whereas the other matrices read $\nabla_{\mathbf{yy}}^2 f_h = \text{diag}(\{\nabla_{\mathbf{y}_i \mathbf{y}_i}^2 f_h\}_{i=1}^n)$ and $\nabla_{\mathbf{y}} \mathbf{h} = \{[\nabla_{\mathbf{y}_i} \mathbf{h}^A \quad \nabla_{\mathbf{y}_i} \mathbf{h}^B]\}_{i=1}^n$, where:

$$\nabla_{\mathbf{y}_i \mathbf{y}_i}^2 f_h = c_i \mathbf{k}^{(i)} = c_i \begin{bmatrix} \mathbf{k}_{\text{sec}}^{(i)} & \begin{matrix} \lambda_1{}^A \sin\theta_i - \lambda_2{}^A \cos\theta_i \\ 0 \end{matrix} \\ \lambda_1{}^A \sin\theta_i - \lambda_2{}^A \cos\theta_i \quad 0 & (\varepsilon_i + 1)(\lambda_1{}^A \cos\theta_i + \lambda_2{}^A \sin\theta_i) \end{bmatrix} \tag{27}$$

$$\nabla_{\mathbf{y}_i} \mathbf{h}^A = c_i \begin{bmatrix} -\cos\theta_i & -\sin\theta_i & 0 \\ 0 & 0 & -1 \\ (\varepsilon_i + 1)\sin\theta_i & -(\varepsilon_i + 1)\cos\theta_i & 0 \end{bmatrix}, \qquad \nabla_{\mathbf{y}_i} \mathbf{h}^B = \begin{bmatrix} 0 & 0 & \cdots & 0 & \cdots & 0 \\ \Theta_{1i} & \Theta_{2i} & \cdots & \Theta_{ii} & \cdots & \Theta_{ni} \\ 0 & 0 & \cdots & 1 & \cdots & 0 \end{bmatrix} \tag{28}$$

Matrix $\mathbf{k}^{(i)}$ can be viewed as an augmented cross-section stiffness matrix, also including rotational variables, whereas $\mathbf{k}_{\text{sec}}^{(i)}$ is given in Eq. (20). Due to its structure, the system of equations in Eq. (26) can be rewritten equivalently as (Luenberger and Ye 2008):

$$\begin{bmatrix} \nabla^2_{\mathbf{yy}} f_h^k & \mathbf{0} & \nabla_{\mathbf{y}} \mathbf{h}^k \\ & \mathbf{0} & \nabla_{\mathbf{q}} \mathbf{h}^k \\ \text{symm.} & & \mathbf{0} \end{bmatrix} \begin{bmatrix} \mathbf{d_y}^k \\ \mathbf{d_q}^k \\ \boldsymbol{\lambda}^{k+1} \end{bmatrix} + \begin{bmatrix} \nabla_{\mathbf{y}} f^k \\ \nabla_{\mathbf{q}} f^k \\ \mathbf{h_{res}}^k \end{bmatrix} = \mathbf{0} \tag{29}$$

Taking into account that constraints $\mathbf{h}^B$ and the last of constraints $\mathbf{h}^A$ are linear, the respective residuals can be set equal to zero. Moreover, the remainders of the residuals, $\nabla_{\mathbf{y}} f^k$ and $\nabla_{\mathbf{q}} f^k$, correspond to the stress resultants and the external forces respectively, that is:

$$\mathbf{h}_{\text{res}} = \begin{bmatrix} q_4 - q_1 - \sum_{i=1}^{n} c_i(\varepsilon_i + 1)\cos\theta_i + L \\ q_5 - q_2 - \sum_{i=1}^{n} c_i(\varepsilon_i + 1)\sin\theta_i \\ \underbrace{\mathbf{0}}_{(n+1)\times 1} \end{bmatrix} \tag{30}$$

$$\nabla_{\mathbf{y}_i} f = c_i \mathbf{D}^{(i)} = c_i \begin{bmatrix} N_i \\ M_i \\ 0 \end{bmatrix} \tag{31}$$

$$\nabla_{\mathbf{q}} f = \mathbf{P} \tag{32}$$

The Hessian in Eq. (29) is a large sparse matrix that contains the second-order information of the element. We can leverage its sparsity in order to avoid a direct inversion, which would encumber the computational procedure. Thereby, we can derive the tangential stiffness matrix $\mathbf{K}$ of the element:

$$\mathbf{K} = \nabla_{\mathbf{q}} \mathbf{h}\, \mathbf{F}^{-1} \nabla_{\mathbf{q}} \mathbf{h}^T \tag{33}$$

where $\mathbf{F}$ = flexibility matrix pertaining to the Lagrange multipliers, which can be determined as follows:

$$\mathbf{F} = \sum_{i=1}^{n} \frac{1}{c_i} \nabla_{\mathbf{y}_i} \mathbf{h}^T (\mathbf{k}^{(i)})^{-1} \nabla_{\mathbf{y}_i} \mathbf{h} \tag{34}$$

As soon as the matrices in Eqs. (33) and (34) have been evaluated, the global stiffness matrix can be easily assembled, as usual, and the nodal displacements and rotation increments $\mathbf{d_q}$ can be computed. The remaining dual and primal unknowns can be then updated for the $k+1$ step, element-wise and section-wise, respectively:

$$\boldsymbol{\lambda}^{k+1} = \boldsymbol{\lambda}_{in}{}^k + (\mathbf{F}^k)^{-1} \nabla_{\mathbf{q}} \mathbf{h}^T \mathbf{d_q}{}^k \tag{35}$$

$$\mathbf{d}_{\mathbf{y}_i}{}^k = -(\mathbf{k}^{(i)k})^{-1} \left(\frac{1}{c_i} \nabla_{\mathbf{y}_i} \mathbf{h}^k \boldsymbol{\lambda}^{k+1} + \mathbf{D}^{(i)k} \right) \tag{36}$$

For the internal Lagrange multipliers $\boldsymbol{\lambda}_{in}$ emerging in Eq. (35), the following relations hold:

$$\boldsymbol{\lambda}_{in} = \mathbf{F}^{-1} \left(\mathbf{h}_{res} - \sum_{i=1}^{n} \nabla_{\mathbf{y}_i} \mathbf{h}^T (\mathbf{k}^{(i)})^{-1} \mathbf{D}^{(i)} \right) \tag{37}$$

$$\nabla_{\mathbf{q}} \mathbf{h} \boldsymbol{\lambda}_{in} = \mathbf{P}_{in} \tag{38}$$

where $\mathbf{P}_{in}$ = internal nodal forces of each member. Technically, the internal nodal forces of the members can assemble the residuals of the entire structure in every iteration, thus being essential in convergence checking and defining the new increment direction of structural displacements and rotations. The whole iteration process can be concisely seen in Algorithm 1 in the form of a procedural pseudocode, where the subscript "str" denotes the corresponding structural vectors and matrices.

Algorithm 1. Hybrid element second order iterative procedure

Initialize $\mathbf{q}_{\text{str}}$, $\boldsymbol{\varepsilon}$, $\boldsymbol{\kappa}$, $\boldsymbol{\lambda}$
For all load steps j
  Set $k = 0$
  Repeat until convergence
    For all members
      For all integration points i
        Compute $\nabla_{\mathbf{y}_i} \mathbf{h}^k$ using Eq. (28)
        Compute tangential stiffness $\mathbf{k}^{(i)k}$ using Eq. (27)
        Compute stress resultants $\mathbf{D}^{(i)k}$ using Eq. (31)
      Compute constraint residuals $\mathbf{h_{res}}{}^k$ using Eq. (30)
      Compute $\mathbf{F}^k$ using Eq. (34)
      Compute $\mathbf{K}^k$ using Eq. (33)
      Compute internal member forces $\mathbf{P_{in}}{}^k$ using Eq. (38)
    Assemble tangential structural stiffness $\mathbf{K}_{str}{}^k$
    Assemble structural internal forces $\mathbf{P_{in,str}}{}^k$
    Set $\mathbf{d_P}{}^k = \mathbf{P_{str}}{}^j - \mathbf{P_{in,str}}{}^k$
    Set $\mathbf{d_{q_{str}}}{}^k = (\mathbf{K_{str}}{}^k)^{-1} \mathbf{d_P}{}^k$
    For all members
      Update Lagrange multipliers $\boldsymbol{\lambda}^{k+1}$ using Eq. (35)
      For all integration points i
        Compute sectional variables increment $\mathbf{d}_{\mathbf{y}_i}{}^k$ using Eq. (36)
        Update sectional variables $\mathbf{y}_i{}^{k+1} = \mathbf{y}_i^k + \mathbf{d}_{\mathbf{y}_i}{}^k$
    Update structural displacements/rotations $\mathbf{q_{str}}{}^{k+1} = \mathbf{q_{str}}{}^k + \mathbf{d_{q_{str}}}{}^k$
  Set $k = k + 1$
  Check convergence

Model Performance Evaluation

Numerical Examples

The proposed model is implemented in four examples based on well-documented benchmark problems in the literature, featuring highly nonlinear responses. The details of each problem can be seen in Fig. 2. Both geometrically nonlinear elastic analyses (GNEAs) and geometrically and materially nonlinear inelastic analyses (GMNIAs) are conducted. The OpenSees software, version 2.5.0, has been selected for validation and comparison purposes because it is open source and incorporates a series of state-of-the-art nonlinear beam-column element concepts in addition to allowing for fiber discretization (Taucer et al. 1991; Spacone et al. 1996; Neuenhofer and Filippou 1997, 1998), as also used herein.

OpenSees analyses were conducted using force-based elements with corotational transformation, 30 fibers, and 5 Gauss-Lobatto integration points in general, whereas 3 integration points were chosen for the densest meshes because, as thoroughly checked, more points do not improve the accuracy in those cases. OpenSees corotational force-based elements allow for geometrically and materially nonlinear analysis assuming moderate rotations and small strains, thus providing a proper baseline for validating the proposed formulation. For the proposed NLP hybrid element, 30 fibers and 5 Gauss-Legendre integration points were chosen, whereas analyses were conducted using the generic arc-length

Problem	P-I	P-II	P-III	P-IV
Name	Cantilever with vertical load	Curling beam	Toggle frame	Lee's frame
References	(De Souza, 2000; Santos & Moitinho de Almeida, 2010; Saje, et al., 1997; Chan, 1988)	(De Souza, 2000; Santos & Moitinho de Almeida, 2010; Schulz & Filippou, 2001; Crisfield, 1990)	(De Souza, 2000; Chan, 1988; Wood & Zienkiewicz, 1977)	(Alemdar & White, 2005; De Souza, 2000; Santos & Moitinho de Almeida, 2010; Cichon, 1984)
Structure	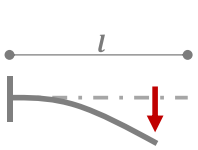	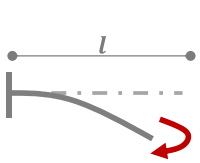	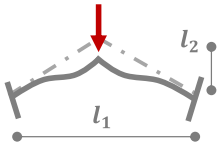	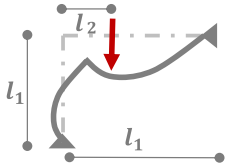
Properties	$l = 0.5$ $d = 0.03$ $E = 200$ $b = 0.03$ $a = 2\%$ $\sigma_y = 2.0$	$l = 0.5$ $d = 0.03$ $E = 200$ $b = 0.03$	$l_1 = 2 \cdot 3.0$ $d = 0.30$ $l_2 = 0.40$ $b = 0.30$ $E = 200$ $\sigma_y = 2.0$ $a = 2\%$	$l_1 = 1.20$ $d = 0.02$ $l_2 = 0.24$ $b = 0.03$ $E = 70.61$ $\sigma_y = 1.02$ $a = 2\%$

Note: l, l_1, l_2 = lengths (m), E = elastic modulus (GPa), d = cross-section height (m), b = cross-section width (m), σ_y = yield strength (GPa), a = inelastic/elastic moduli ratio for bilinear elastoplastic material with linear kinematic hardening.

Fig. 2. Example problems description.

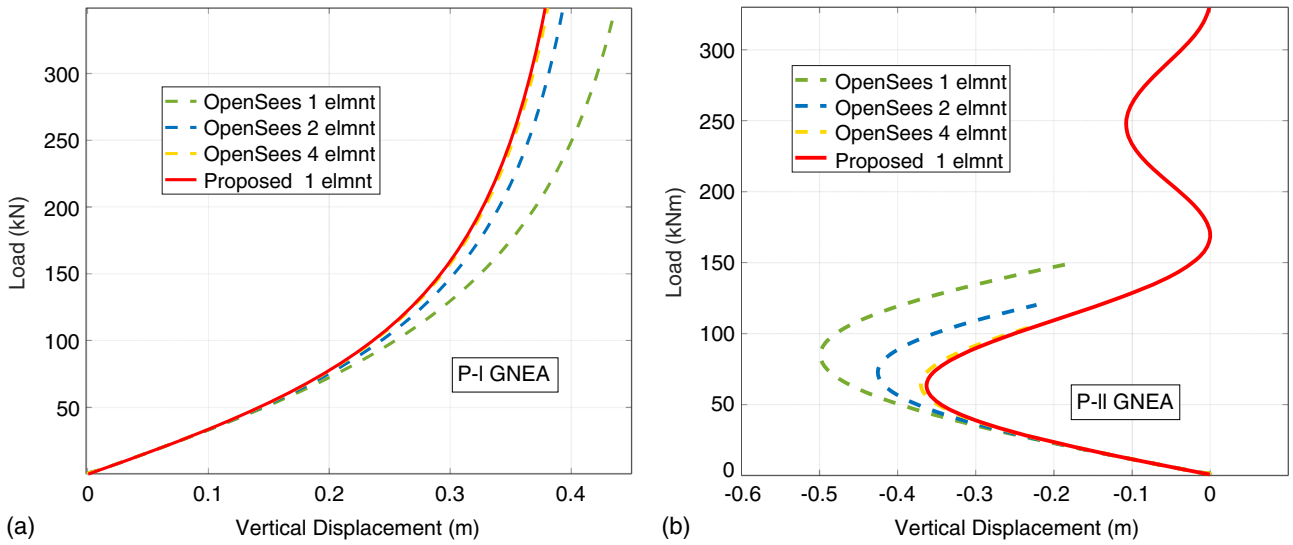

Fig. 3. GNEA results for problems: (a) P-I; and (b) P-II.

scheme (Crisfield 1981) when snapping behaviors appeared. All analyses were executed in 100 pseudotime steps. Results for all problem cases of Fig. 2 are demonstrated in Figs. 3–5. The vertical displacements in the figures correspond to the loaded node, as illustrated in Fig. 2.

In problem P-I, the response of a cantilever imposed to an incremental vertical load at the free edge is investigated for both the GNEA and GMNIA cases. A special feature of this problem is that as the external force increases, the nonlinear solution deviates considerably from the linear branch because extreme rotations of the cross-sections gradually activate increased axial resistance. This membrane function of the member can considerably enhance the bending stiffness, which is the only one taken into account by geometrically linear assumptions, and the capability of a model capturing such mechanisms is particularly desirable in progressive collapse problems, as discussed previously.

In P-II, the same cantilever as in the previous example is loaded with a concentrated bending moment at the free edge. This structure is also known as the curling beam because this tip moment deforms the structure in a curling fashion. The problem is examined within the elastic regime because it exhibits extremely large rotations and displacements. Equilibrium at every position enforces that the moment is constant within the element and thus curvature should be constant too. This means that the deformed shape is a circular arc with radius equal to the inverse curvature. Due to its unusual response, this problem reveals some limitations and inconsistencies emanating from corotational formulations.

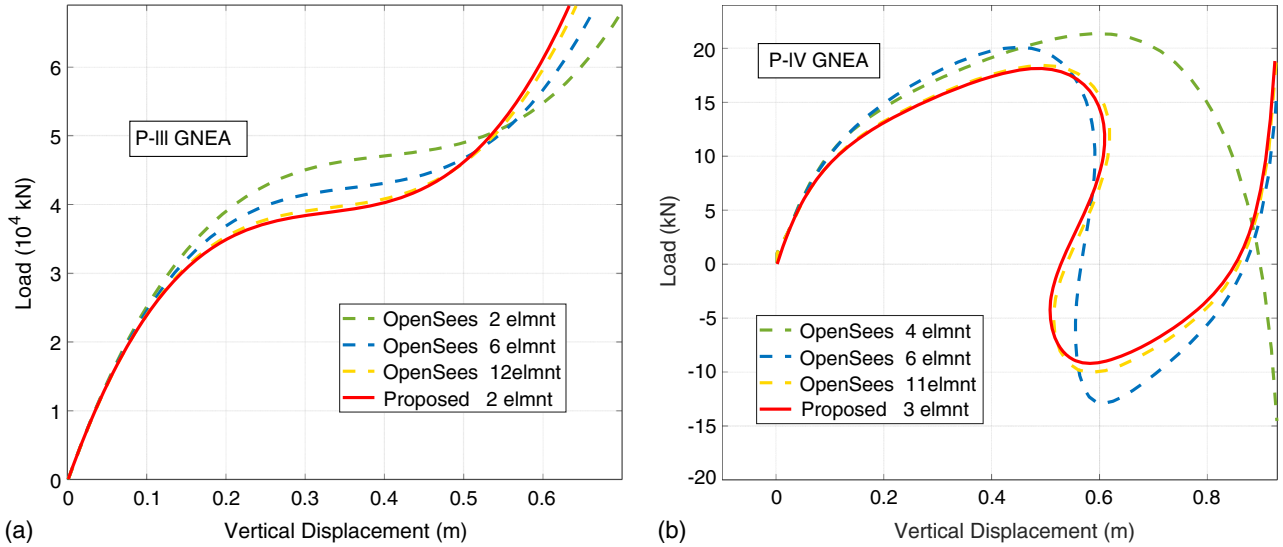

Fig. 4. GNEA results for problems: (a) P-III; and (b) P-IV.

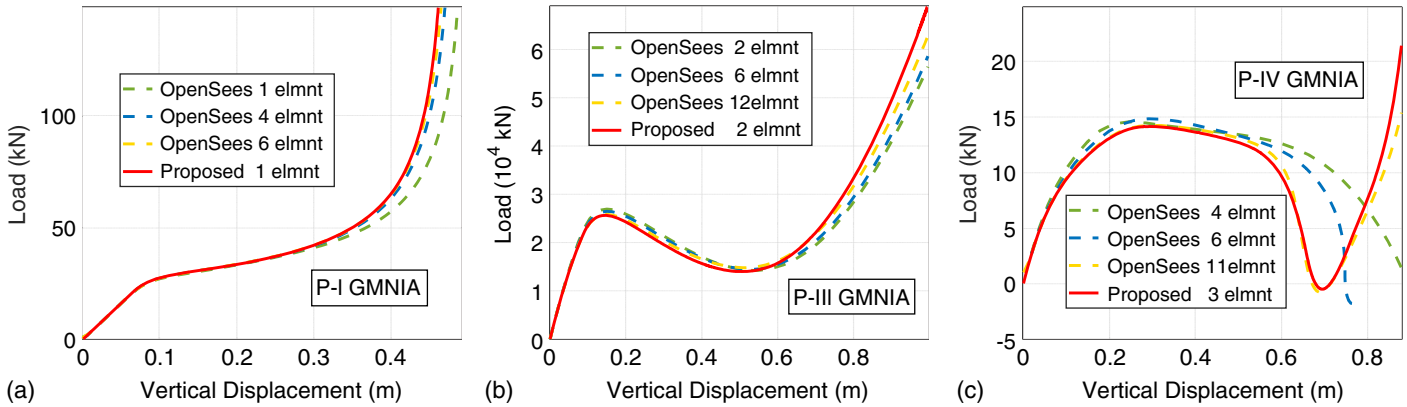

Fig. 5. GMNIA results for problems: (a) P-I; (b) P-III; and (c) P-IV.

Example P-III studies the toggle frame structure which is a well known nonlinear problem. This structure is usually modeled with truss elements, however, in this investigation, the developed beam elements are used. The nonlinear feature of interest in this case is that the obtained equilibrium path often exhibits a snap-through behavior, which indicates a forceful buckling of the two intersecting members. The inelastic snapping behavior of the frame is also studied, as seen in Fig. 5.

Problem P-IV investigates the nonlinear response of Lee's frame. This is an inverse L-shaped frame, pinned at the edges, eccentrically loaded near the intersection of the two members, as shown in Fig. 2. Due to its structural geometry and eccentricity of the external loading, this structure exhibits a highly nonlinear behavior, which has rich implications in relation to the efficacy of the proposed element formulation and exhibits peculiar snapping responses both in the elastic and inelastic cases.

As shown in Figs. 3 and 5, problem P-I is accurately solved with one proposed element in both GNEA and GMNIA. In GNEA, OpenSees eventually requires four force-based elements to attain comparable accuracy, whereas in GMNIA the required discretization in OpenSees rises to six elements, as illustrated in Fig. 5. The solution of P-III, presented in Figs. 4 and 5, requires a noteworthy increase in the total number of force-based elements, whereas the proposed formulation is accurate with only one element per member in both cases.

Problem P-IV also requires fine discretization in OpenSees, both in GNEA and GMNIA, as can be seen in Figs. 4 and 5. OpenSees results using three force-based elements, that is, one element per member, as used in our developed approach, bear no resemblance to the actual solution and have been discarded. Even in the case of 4 elements, results are largely inaccurate in strongly nonlinear regimes and correct path is eventually reached only when the structure is discretized with 11 elements. For GMNIA, OpenSees notably stops before reaching the final 100th step, when six elements are used. Premature analysis termination is an important and alarming issue, especially for large, computationally intensive problems.

This phenomenon also occurs, even more severely, in the analysis results of example P-II, shown in Fig. 3. In this problem, OpenSees stops prematurely in all cases, even when it is on the right solution path (with four elements), and fails to provide any solution in highly nonlinear regions. The issue of nonconvergence is not circumvented here in OpenSees, even in the presence of a denser mesh discretization, with more than four elements, and analysis results do not provide information about extreme loading levels.

In nonlinear analysis, nonconvergence of the algorithm is usually regarded as failure of the structural system, but, as seen in this exaggerated example, this assumption can be inaccurate, implying failure indicator definitions that are metrics of algorithmic insufficiencies rather than response demands.

Competitive performance has been also showcased in a number of prior works in the literature that suggested different finite element formulations, with the most indicative ones being listed in Fig. 2 as well. The flexibility-based element developed in De Souza (2000) reaches comparable performance to our proposed element, requiring coarse discretization of one element per member in the majority of problems, whereas geometrically exact formulations in Santos and Moitinho de Almeida (2010) and Saje et al. (1997) also succeed in capturing accurate responses with low number of elements. Other approaches (Schulz and Filippou 2001) and earlier ones (Wood and Zienkiewicz 1977; Cichon 1984; Chan 1988; Crisfield 1990), although not avoiding denser meshes, exhibit accurate responses in problems with highly nonlinear equilibrium paths. All benchmark problems examined in this work feature at most three members, however, as indicated by the generic form of Algorithm 1, the suggested formulation can be straightforwardly applied to more complex 2D structural problems, such as the ones presented in Santos (2011).

Overall, in all the examined examples, the proposed approach manifests notable algorithmic strengths because it (i) maintains coarse meshing demands even in arduous nonlinear problems; (ii) captures accurately the nonlinear behavior of the modeled structural systems; (iii) reduces the total DOF even for small structures, boosting computational speed; and (iv) exhibits robust algorithmic performance in poorly convergent regions.

Discussion on Complexity

The proposed NLP hybrid element formulation introduces additional variables in comparison to standard formulations through the use of Lagrange multipliers and rotational components at the integration points. The latter are numerically treated as an extension over the standard sectional variables, and the new sectional vector of unknowns lies now in $\mathbb{R}^3$ instead of the typical $\mathbb{R}^2$. This extension adds a negligible computational cost because cross-section derivations are processed independently of each other. Additionally, in the overall structural level, the time for updating the sectional variables remains linear with the number of elements and integration points per element.

The Lagrange multipliers essentially define an augmented space of dual forces, which can be mapped back to the external nodal elemental forces, as shown in Eq. (23). These additional dual variables are processed element-wise, which technically means that they correspond to solely elemental entities. They are analogous to the corotational nodal forces in the flexibility-based formulations, which are meaningful only on an elemental level, evaluated independently. Within the flexibility-based formulations for plane structures, this vector of forces lies in $\mathbb{R}^3$, whereas in the present formulation it is in $\mathbb{R}^{3+n}$. As such, the inversion of the corresponding flexibility matrix presented in Eq. (34) is apparently more cumbersome than the inversion of a (3×3) matrix. However, under the reasonable assumption that integration points per element are more or less constant, say, 3–8 in the vast majority of applications, we end up again with a linear processing time related to the number of elements.

Most importantly, as clearly supported by the numerical example results, these additional variables relate to a minor element-wise computational overhead, which eventually reduces the overall required structural DOFs drastically. For an assumed level of accuracy, an important reduction in the number of elements and, as a consequence, in the dimensions of the global structural stiffness matrix is achieved. This is a significant result because the inversion of the global stiffness matrix is the dominant computational hurdle of the iterative procedure, especially as the problem size gets bigger, because its computational time is cubic to the number of DOFs, with standard approaches. In a more schematic description, the presented formulation decentralizes an important part of the computational effort, to be carried out locally and independently by each element. Therefore, the required computational demands for updating the global information related to the entire structural system are significantly reduced.

In Fig. 6, the total number of variables for the solved problems P-I through P-IV are presented per level of processing, namely sectional, elemental, and structural, and are compared with the OpenSees flexibility-based elements. Comparison corresponds only to those analyses that provided related equilibrium paths in the previously examined problems (continuous and converged dashed lines in Figs. 3–5), thus considering three integration points for the flexibility-based elements and five for the proposed one, as already explained. It is obvious that in all cases, due to the reduced discretization, the total number of variables to be updated in every iteration is significantly reduced, despite the presence of the newly

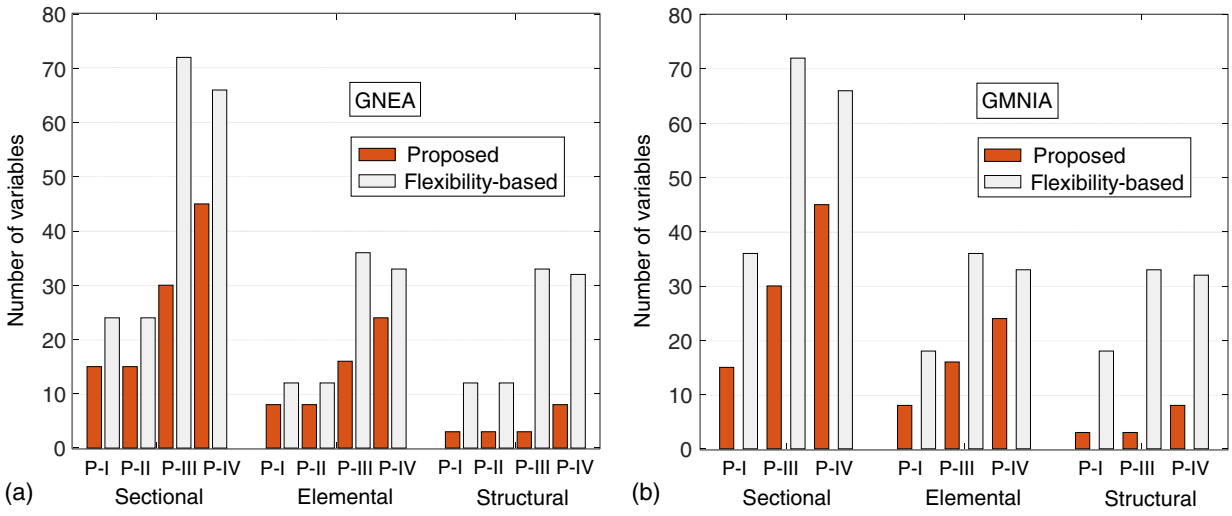

Fig. 6. Number of sectional, elemental, and structural variables in all numerical examples.

introduced variables at the sectional and elemental levels by the proposed formulation. Especially at the structural level, a significant reduction of variables is accomplished, indicating reduced structural stiffness matrix dimensions and thus required computational effort at each iteration.

Conclusions

A new hybrid beam-column element based on a nonlinear programming formulation is presented in this work, able to circumvent various issues emerging in highly nonlinear structural simulations. The suggested methodology allows for accuracy, coarse discretization, computational speed, and algorithmic robustness. Exact kinematic fields are used, kinematic compatibility constraints are attached to the total potential energy functional through Lagrange multipliers, and structural analysis is originally treated as a NLP problem, seeking optima in terms of the resulting hybridized energy functional. This formulation integrates the philosophy of nonlinear structural analysis with NLP concepts, thus allowing structural analysis to take advantage of the abundance of sophisticated methods in the NLP field. The model is validated through benchmark problems featuring extreme geometrical and material nonlinearities, and it showcases superior results compared to standard force-based elements. The robust algorithmic performance of the proposed element, even in large inelastic displacement problems, and its abilities for coarse discretization without reducing accuracy or exploding DOF dimensions are essential properties that enable high-performance nonlinear structural simulations without any need for the usually applied corotational approaches. Overall, the proposed NLP hybrid element offers a versatile computational model that can facilitate improved and realistic failure limit state definitions that are not abstract proxies of failure indicators or, even worse, metrics of numerical analysis limitations.

Acknowledgments

This material is based upon work supported by the National Science Foundation under Grant No. 1634575. The first two authors gratefully acknowledge this support.

References

Alemdar, B. N., and D. W. White. 2005. "Displacement, flexibility, and mixed beam-column element formulations for distributed plasticity analysis." *J. Struct. Eng.* 131 (12): 1811–1819. https://doi.org/10.1061/(ASCE)0733-9445(2005)131:12(1811).

Andriotis, C. P., I. Gkimousis, and V. K. Koumousis. 2015. "Modeling reinforced concrete structures using smooth plasticity and damage models." *J. Struct. Eng.* 142 (2): 04015105. https://doi.org/10.1061/(ASCE)ST.1943-541X.0001365.

Andriotis, C. P., and K. G. Papakonstantinou. 2018. "Extended and generalized fragility functions." *J. Eng. Mech.* 144 (9): 04018087. https://doi.org/10.1061/(ASCE)EM.1943-7889.0001478.

Argyris, J. H., S. Kesley, and H. Kamel. 1964. *Matrix methods of structural analysis: A precis of recent developments*. Oxford, UK: Pergamon Press.

Au, S. K., and J. L. Beck. 2001. "Estimation of small failure probabilities in high dimensions by subset simulation." *Probab. Eng. Mech.* 16 (4): 263–277. https://doi.org/10.1016/S0266-8920(01)00019-4.

Baker, J. W. 2015. "Efficient analytical fragility function fitting using dynamic structural analysis." *Earthquake Spectra* 31 (1): 579–599. https://doi.org/10.1193/021113EQS025M.

Bathe, K.-J., and S. Bolourchi. 1979. "Large displacement analysis of three dimensional beam structures." *Int. J. Mech. Sci.* 14 (7): 961–986. https://doi.org/10.1002/nme.1620140703.

Bazaraa, M. S., H. D. Sherali, and C. M. Shetty. 2006. *Nonlinear programming*. 3rd ed. Hoboken, NJ: Wiley.

Chan, S. L. 1988. "Geometric and material non-linear analysis of beam-columns and frames using the minimum residual displacement method." *Int. J. Numer. Methods Eng.* 26 (12): 2657–2669. https://doi.org/10.1002/nme.1620261206.

Cichon, C. 1984. "Large displacements in-plane analysis of elastic-plastic frames." *Comput. Struct.* 19 (5–6): 737–745. https://doi.org/10.1016/0045-7949(84)90173-1.

Crisfield, M. A. 1981. "A fast incremental/iterative solution procedure that handles 'snap-through'." *Comput. Struct.* 13 (1–3): 55–62. https://doi.org/10.1016/0045-7949(81)90108-5.

Crisfield, M. A. 1990. "A consistent co-rotational formulation for non-linear, three dimensional beam elements." *Comput. Methods Appl. Mech. Eng.* 81 (2): 131–150. https://doi.org/10.1016/0045-7825(90)90106-V.

Crisfield, M. A. 1997. *Non-linear finite element analysis of solids and structures*. Chichester, UK: Wiley.

De Borst, R., M. A. Crisfield, J. J. C. Remmers, and C. V. Verhoosel. 2012. *Nonlinear finite element analysis of solids and structures*. Chichester, UK: Wiley.

De Souza, R. 2000. "Force-based finite element for large displacement inelastic analysis of frames." Ph.D. dissertation, Univ. of California, Berkeley.

Felippa, C. A. 1994. "A survey of parametrized variational principles and applications to computational mechanics." *Comput. Methods Appl. Mech. Eng.* 113 (1–2): 109–139. https://doi.org/10.1016/0045-7825(94)90214-3.

Felippa, F. C., and B. Haugen. 2005. "A unified formulation of small-strain corotational finite elements. I: Theory." *Comput. Methods Appl. Mech. Eng.* 194 (21–24): 2285–2335. https://doi.org/10.1016/j.cma.2004.07.035.

Gerasimidis, S., G. Deodatis, T. Kontoroupi, and M. Ettouney. 2015. "Loss-of-stability induced progressive collapse modes in 3D steel moment frames." *Struct. Infrastr. Eng.* 11 (3): 334–344. https://doi.org/10.1080/15732479.2014.885063.

Hjelmstad, K. D., and E. Taciroglu. 2003. "Mixed variational methods for finite element analysis of geometrically non-linear, inelastic Bernoulli-Euler beams." *Commun. Numer. Methods Eng.* 19 (10): 809–832. https://doi.org/10.1002/cnm.622.

Izzuddin, B. A., A. G. Vlassis, A. Y. Elghazouli, and D. A. Nethercot. 2008. "Progressive collapse of multi-storey buildings due to sudden column loss. I: Simplified assessment framework." *Eng. Struct.* 30 (5): 1308–1318. https://doi.org/10.1016/j.engstruct.2007.07.011.

Luenberger, D. G., and Y. Ye. 2008. *Linear and nonlinear programming*. 3rd ed. New York: Springer.

Neuenhofer, A., and F. C. Filippou. 1997. "Evaluation of nonlinear frame finite-element models." *J. Struct. Eng.* 123 (7): 958–966. https://doi.org/10.1061/(ASCE)0733-9445(1997)123:7(958).

Neuenhofer, A., and F. C. Filippou. 1998. "Geometrically nonlinear flexibility-based frame finite element." *J. Struct. Eng.* 124 (6): 704–711. https://doi.org/10.1061/(ASCE)0733-9445(1998)124:6(704).

Reissner, E. 1972. "On one-dimensional finite-strain beam theory: The plane problem." *J. Appl. Math. Phys. (ZAMP)* 23 (5): 795–804. https://doi.org/10.1007/BF01602645.

Saje, M., I. Planinc, G. Turk, and B. Vratanar. 1997. "A kinematically exact finite element formulation of planar elastic-plastic frames." *Comput. Methods Appl. Mech. Eng.* 144 (1–2): 125–151. https://doi.org/10.1016/S0045-7825(96)01172-3.

Santos, H. 2011. "Complementary-energy methods for geometrically nonlinear structural models: An overview and recent developments in the analysis of frames." *Arch. Comput. Methods Eng.* 18 (4): 405–440. https://doi.org/10.1007/s11831-011-9065-6.

Santos, H., P. Pimenta, and J. Almeida. 2011. "A hybrid-mixed finite element formulation for the geometrically exact analysis of three-dimensional framed structures." *Comput. Mech.* 48 (5): 591–613. https://doi.org/10.1007/s00466-011-0608-3.

Santos, H. A. F. A., and J. P. Moitinho de Almeida. 2010. "Equilibrium-based finite-element formulation for the geometrically exact analysis of planar framed structures." *J. Eng. Mech.* 136 (12): 1474–1490. https://doi.org/10.1061/(ASCE)EM.1943-7889.0000190.

Saritas, A., and F. Filippou. 2009. "Inelastic axial-flexure-shear coupling in a mixed formulation beam finite element." *Int. J. Non Linear Mech.* 44 (8): 913–922. https://doi.org/10.1016/j.ijnonlinmec.2009.06.007.

Schulz, M., and F. C. Filippou. 2001. "Non-linear spatial Timoshenko beam element with curvature interpolation." *Int. J. Numer. Methods Eng.* 50 (4): 761–785. https://doi.org/10.1002/1097-0207(20010210)50:4<761::AID-NME50>3.0.CO;2-2.

Sivaselvan, M. V., and A. M. Reinhorn. 2006. "Lagrangian approach to structural collapse simulation." *J. Eng. Mech.* 132 (8): 795–805. https://doi.org/10.1061/(ASCE)0733-9399(2006)132:8(795).

Soydas, O., and A. Saritas. 2013. "An accurate nonlinear 3D Timoshenko beam element based on Hu-Washizu functional." *Int. J. Mech. Sci.* 74: 1–14. https://doi.org/10.1016/j.ijmecsci.2013.04.002.

Spacone, E., V. Ciampi, and F. C. Filippou. 1996. "Mixed formulation of nonlinear beam finite element." *Comput. Struct.* 58 (1): 71–83. https://doi.org/10.1016/0045-7949(95)00103-N.

Stolarski, H., and T. Belytschko. 1983. "Shear and membrane locking in curved C^0 elements." *Comput. Methods Appl. Mech. Eng.* 41 (3): 279–296. https://doi.org/10.1016/0045-7825(83)90010-5.

Taucer, F. F., E. Spacone, and F. C. Filippou. 1991. *A fiber beam-column element for seismic response analysis of reinforced concrete structures*. Rep. No. UCB/EERC-91/17. Berkeley, CA: Earthquake Engineering Research Center, Univ. of California.

Taylor, R., F. Filippou, A. Saritas, and F. Auricchio. 2003. "A mixed finite element method for beam and frame problems." *Comput. Mech.* 31 (1): 192–203. https://doi.org/10.1007/s00466-003-0410-y.

Wood, R. D., and O. Zienkiewicz. 1977. "Geometrically nonlinear finite element analysis of beams, frames, arches, and axisymmetric shells." *Comput. Struct.* 7 (6): 725–735. https://doi.org/10.1016/0045-7949(77)90027-X.

Zeris, C., and S. A. Mahin. 1988. "Analysis of reinforced concrete beam-columns under uniaxial excitation." *J. Struct. Eng.* 114 (4): 804–820. https://doi.org/10.1061/(ASCE)0733-9445(1988)114:4(804).

Zhang, R., and H. Zhong. 2013. "Weak form quadrature element analysis of planar slender beams based on geometrically exact beam theory." *Arch. Appl. Mech.* 83 (9): 1309–1325. https://doi.org/10.1007/s00419-013-0748-3.